

Functionalized polyamide membranes yield suppression of biofilm and planktonic bacteria while retaining flux and selectivity

Original

Functionalized polyamide membranes yield suppression of biofilm and planktonic bacteria while retaining flux and selectivity / Dadashi Firouzjaei, M.; Pejman, M.; Gh, M. S.; Aktij, S. A.; Zolghadr, E.; Rahimpour, A.; Sadrzadeh, M.; Shamsabadi, A. A.; Tiraferri, A.; Elliott, M.. - In: SEPARATION AND PURIFICATION TECHNOLOGY. - ISSN 1383-5866. - 282:(2022), p. 119981. [10.1016/j.seppur.2021.119981]

Availability:

This version is available at: 11583/2950993 since: 2022-01-18T14:54:42Z

Publisher:

Elsevier B.V.

Published

DOI:10.1016/j.seppur.2021.119981

Terms of use:

This article is made available under terms and conditions as specified in the corresponding bibliographic description in the repository

Publisher copyright

(Article begins on next page)

1
2 **Functionalized Polyamide Membranes Yield Suppression of Biofilm and**
3 **Planktonic Bacteria while Retaining Flux and Selectivity**

4
5 Mostafa Dadashi Firouzjaei ^{[a]1}, Mehdi Pejman ^{[b]1}, Mohammad Sharifian Gh.^[c], Sadegh
6 Aghapour Aktij^[d,e], Ehsan Zolghadr ^[a,f], Ahmad Rahimpour*^[b,g], Mohtada Sadrzadeh^[d], Ahmad
7 Arabi Shamsabadi ^[h], Alberto Tiraferri *^[b], and Mark Elliott*^[a]

8
9 ^[a] Department of Civil, Environmental and Construction Engineering, University of Alabama,
10 Tuscaloosa, AL, 35487, USA

11 ^[b] Department of Environment, Land and Infrastructure Engineering (DIATI), Politecnico di
12 Torino, Corso Duca degli Abruzzi 24, 10129 Turin, Italy

13 ^[c] Department of Cell Biology, University of Virginia, Charlottesville, VA 22908, United States

14 ^[d] Department of Mechanical Engineering, 10-367 Donadeo Innovation Center for Engineering,
15 Advanced Water Research Lab (AWRL), University of Alberta, Edmonton, AB, T6G 1H9,
16 Canada

17 ^[e] Department of Chemical & Materials Engineering, University of Alberta, Edmonton, AB T6G
18 1H9, Canada

19 ^[f] Department of Physics and Astronomy, University of Alabama, Tuscaloosa, AL 35487, USA

20 ^[g] Department of Applied Science and Technology, Politecnico di Torino, Corso Duca Degli
21 Abruzzi 24, 10129, Turin, Italy

22 ^[h] Department of Chemistry, University of Pennsylvania, Philadelphia, Pennsylvania 19104,
23 United States

24
25
26
27
28
29
30
31
32
33
34
35

*Corresponding authors:

Mark Elliott (melliott@eng.ua.edu)

Ahmad Rahimpour (ahmad.rahimpour@polito.it)

Alberto Tiraferri (alberto.tiraferri@polito.it)

¹ The authors contributed equally to this work.

36 **ABSTRACT**

37 Biofouling is a major challenge for desalination, water treatment, and water reuse
38 applications using polymer-based membranes. Two classes of novel silver-based metal azolate
39 frameworks (MAF) are proposed to decorate polyamide (PA) forward osmosis membranes and to
40 improve numerous aspects of fouling and transport. Membranes functionalized with two
41 concentrations of each MAF are compared with a pristine control material, with results that
42 clearly highlight their tunability and bio-inhibitory effects. We report for the first time PA
43 membranes yielding near complete suppression of a robust biofilm-forming bacterium
44 (*Pseudomonas aeruginosa*) and inactivation of planktonic bacteria, while maintaining high
45 selectivity. These features improve the long-term water flux performance of the membranes,
46 tested during 24 hours of accelerated biofouling and organic fouling conditions, and showing
47 lower than 10% and 20% decline in water flux. These enhancements were achieved with only
48 0.03% to 0.06% mass of additives and little generation of hazardous waste products, indicating
49 that low-cost and environmentally benign functionalization can prevent biofouling growth while
50 maintaining selectivity and transport for high-performance desalination, water treatment and
51 reuse.

52 **Keywords:** biofilm inhibition; desalination; water treatment; metal azolate framework;
53 antibacterial membranes

54

55 INTRODUCTION

56 Biofilms are ensembles of microorganisms that develop upon attachment to surfaces and
57 that possess biochemical properties, phenotypic characteristics, and architectures distinct from
58 their planktonic and free-swimming counterparts.[1] One of the most important characteristics of
59 biofilms is their antibiotic resistance, which can be up to 1,000-times greater than that of common
60 planktonic cells.[2] This specific property of biofilms is a major challenge for numerous
61 industrial and medical fields.[3] *Pseudomonas aeruginosa* (*P. aeruginosa*) is one such highly-
62 resistant, biofilm-forming bacterial species[4] and is one of the twelve priority pathogens listed
63 by WHO.[5] What further hinders the successful inhibition of this bacterium is that through
64 formation of biofilms, the resistance of *P. aeruginosa* is increased by a self-made protector
65 environment against treatments and host immune defense.[6] There are many studies aimed at
66 mitigating *P. aeruginosa* biofilm formation, but not much success in fully preventing the growth
67 of these communities.[7] Moreover, most of the approaches are not sufficiently reproducible, lack
68 technical validity, or both.[8]

69 Microorganisms are ubiquitous in the environment and controlling or preventing the
70 colonization of surfaces and the growth of biofilms are major challenges for many industries,
71 including those engaged in healthcare, food production, and water treatment.[9] In particular,
72 biofouling has been called the “Achilles’ Heel” of membrane-based water treatment[10], causing
73 numerous adverse effects including compromised membrane integrity, resistance to water flux,
74 and deterioration of water quality.[11,12] Control of biofilm formation and removal of existing
75 biofilms is often attempted using remedial actions, such as scouring or disinfection.[13]
76 Unfortunately, polymer-based membranes provide a hospitable environment for biofilm
77 formation, especially when treating nutrient-rich waters[14], and they can be easily damaged by

78 the oxidants commonly used to control biofilm growth.[15] Altering the surface properties of the
79 membrane by increasing hydrophilicity, reducing roughness, and imparting negative surface
80 charge can reduce bacterial attachment and growth.[11] Additionally, incorporation of
81 antimicrobial agents into the membrane surface layer has shown particular promise in mitigating
82 the initial establishment and subsequent growth of biofilms.[16–18]

83 Recent studies have demonstrated some success in controlling biofilm growth and
84 improving water flux through functionalization of membrane surfaces with antimicrobial metal-
85 organic frameworks.[17,19,20] However, most of these studies have shown only moderate
86 improvements in bacterial inactivation, suppression of biofilm, and maintenance of water
87 flux.[17,19,20] Additionally, these studies typically investigated bacteria that do not tend to form
88 robust biofilms, for example, *Escherichia coli* (*E. coli*).

89 In this study, we fabricated novel thin-film nanocomposite (TFN) polyamide (PA)
90 membranes decorated with silver-based metal-azolate framework (MAF) nanoparticles (NPs).
91 We tested two different organic linkers of the MAF crystals, namely, 2-methylimidazole and
92 benzimidazole, both of which are hypothesized to be seamlessly incorporated within the PA
93 matrix. Both linkers also possess antimicrobial properties of their own, thus potentially increasing
94 the antimicrobial properties of the MAFs.[21,22] We engineered the polyamide surface following
95 the principle of atom economy, thus maximizing the density of MAF starting from dispersion
96 with NP concentrations of only 0.03 and 0.06 wt.%. Low concentration of additives reduces cost
97 and increases the feasibility of commercial application.

98 While a number of approaches to incorporate antimicrobial agents have been successful in
99 partially controlling biofouling and flux reduction, our objective is to provide the first
100 demonstration of all of the following features simultaneously: (i) inactivation of planktonic

101 bacteria, (ii) nearly complete suppression of the growth of a relevant and robust biofilm-forming
102 organism (*P. aeruginosa*), and (iii) retention of flux under simulation of long-term organic
103 fouling and biofouling with a high degree of selectivity. Additionally, this membrane
104 functionalization is achievable through a facile process with low-concentration additives, making
105 this process potentially scalable.

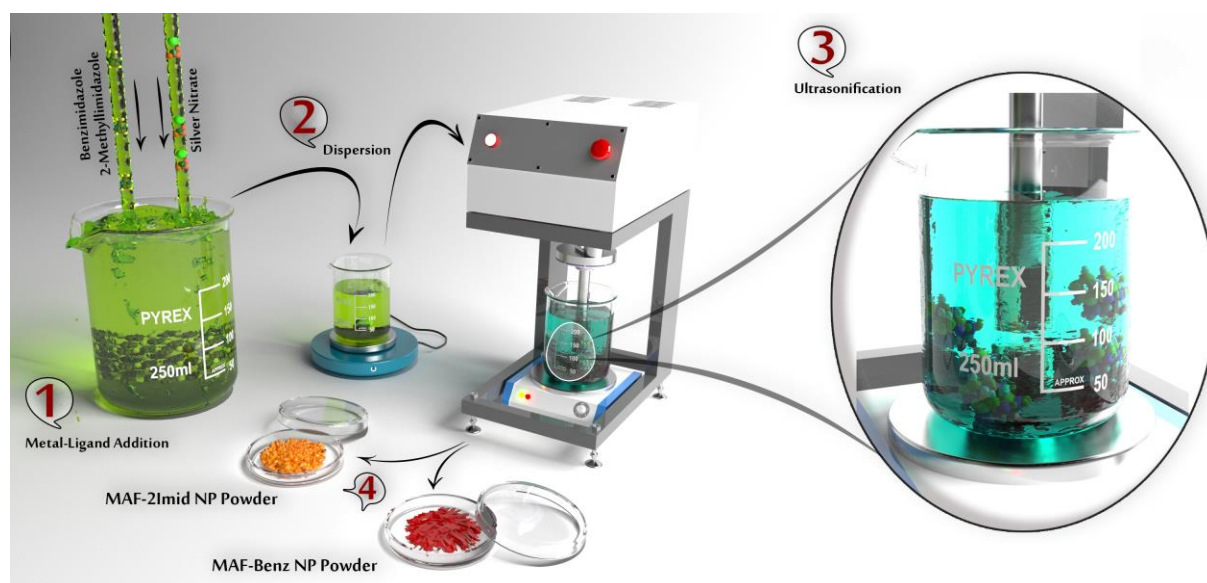
106 **METHODS**

107 **Materials and Chemicals.** Poly (ether sulfone) (PES, M_w of 58,000 g/mol) was
108 purchased from BASF, Germany. Poly (vinylpyrrolidone) (PVP M_w of 25,000 g/mol), N,N-
109 dimethylformamide (DMF), 1,3-phenylenediamine (MPD), n-hexane, trimesoyl chloride (TMC),
110 sodium chloride (NaCl), silver nitrate ($AgNO_3$), benzimidazole, 2-methylimidazole, and ethanol
111 were purchased from Merck, Germany. Sodium dodecyl sulfate (SDS) and propidium iodide
112 were acquired from Sigma-Aldrich.

113 **Synthesis and Characterization of Ag-MAF Nanoparticles.** The metal solution was
114 prepared by dispersion of 0.17 g of $AgNO_3$ in water (30 mL). The ligand solutions were prepared
115 separately by dissolving 0.082 g of 2-methylimidazole in 30 mL of ethanol and 0.118 g of
116 benzimidazole in 40 mL of ethanol, respectively. Ligand and metal solutions were sonicated for 2
117 min, then mixed at room temperature and stirred for 30 min. The precipitate was then collected,
118 washed with deionized water and ethanol five times, and finally, air-dried. The silver azolate
119 frameworks comprising 2-methylimidazole ligand are labeled MAF-2Imid, while the MAFs
120 consisting of benzimidazole are labeled MAF-Benz. **Figure 1** schematically shows the Ag-MAF
121 synthesis steps.

122 **Characterization of the Nanoparticles.** Attenuated total reflectance-FTIR (ATR-FTIR
123 spectroscopy (Varian Excalibur FTS-3000) was used to study the functional groups of the MAFs

124 structures. To determine the crystalline structure of MAFs, X-ray powder diffraction (XRD)
125 spectra were obtained at 298 K, 40 mA and 40 kV with an XPERT-PRO X-ray diffractometer
126 equipped with a Cu-K α radiation source ($\lambda=1.5406\text{\AA}$). Transmission electron microscopy (TEM)
127 (Zeiss EM900) and field emission scanning electron microscopy (FE-SEM) (MIRA3 TESCAN)
128 equipped with energy-dispersive X-ray spectroscopy (EDX) were applied to analyze the
129 morphology of the MAF samples. The average size distributions of MAF NPs were investigated
130 with dynamic light scattering (DLS) (Nano ZS ZEN 3600). X-ray photoelectron spectroscopy
131 (XPS) (Bestec, Germany) equipped with a 100 μm monochromatic Al-K α X-ray photoelectron
132 spectrometer source was applied to identify the characteristic elements of the MAF structures.



133
134 **Figure 1.** Schematic illustration of MAF-Benz and MAF-2imid fabrication procedure. Steps 1, 2 involved metal and ligand
135 individual dispersion followed by mixing of the two solutions; these steps were followed by (3) ultrasonification and (4) final
136 powder washing and drying.

137 **Membrane Functionalization.** Surface modification was carried out by incorporation of
138 MAF-2Imid and MAF-Benz NPs in the surface layer of the membrane. The TFC FO membrane
139 fabrication included two steps. First, a PES ultrafiltration support layer was fabricated by non-
140 solvent-induced phase separation (NIPS). The PES solution (14 wt.% PES and 86 wt.% DMF)
141 was cast on a clean glass plate with a casting knife (100 μm gate height) followed by immersion

142 in a water coagulation bath at room temperature. Second, the PA active layer was formed by
143 interfacial polymerization (IP) on top of the PES support. To this purpose, the PES support
144 membrane was taped onto a glass plate and then immersed in 30 mL of MPD aqueous solution
145 (2.0 wt.%) for 2 min. The excess MPD solution was removed from the PES membrane surface
146 using an air knife. Then, the membrane was immersed in a 0.1 wt.% TMC solution (hexane) for
147 30 s. The membranes were then heat-cured at 80 °C for 5 min. This procedure resulted in a
148 pristine (blank) TFC membrane, used for control experiments.

149 For the fabrication of the TFN membranes, the same procedure was followed, except 0.03 or
150 0.06 wt.% of MAF-2Imid and MAF-Benz NPs were separately dispersed in the MPD solution.
151 The mixture of MPD and NPs were sonicated for 20 min in an ice-bath before use. The TFN
152 membranes are referred to as Ag-2Imid-3 (0.03% wt.% of MAF-2Imid), Ag-2Imid-6 (0.06%
153 wt.% of MAF-2Imid), Ag-Benz-3 (0.03% wt.% of MAF-Benz), Ag-Benz-6 (0.06% wt.% of
154 MAF-Benz).

155 **Membrane Characterization.** Thermo Scientific™, Apreo, scanning electron
156 microscope equipped with an EDX detector was applied to characterize the surface and cross-
157 sectional morphologies of the membranes. Atomic force microscopy (AFM, EasyScan II, Swiss)
158 was used to determine their surface roughness. To minimize the experimental error, the surface
159 roughness was determined for three separate membranes. The surface chemistry of the
160 membranes was analyzed by ATR-FTIR (Thermo Scientific USA). The surface charge was
161 assessed with a SurPASS electrokinetic solid surface zeta potential analyzer (Anton Paar USA,
162 Ashland, VA). All the streaming potential measurements were conducted in a background
163 electrolyte solution of 1 mM KCl at 25 °C, over a pH range of 4-9. The zeta potentials of the
164 membranes were calculated based on the Helmholtz-Smoluchowski equation. Two separate

165 samples of each membrane were assessed to account for experimental error. The membrane
166 surface wettability was assessed by means of contact angle measurements (Dataphysics, OCA 15
167 plus), whereby an average value was calculated from measurements at five random positions. The
168 elemental composition and chemical bonding information of the membrane surface, as well as the
169 release of silver ions from the membrane structure, were evaluated with X-ray photoelectron
170 spectroscopy (XPS, Bestec, Germany).

171 **Measurements of Transport, Fouling, and Biofouling Behavior.** The solute
172 permeability (B) and water permeability (A) coefficients, as well as the antifouling and anti-
173 biofouling properties of the membranes, were evaluated with an FO setup following the protocol
174 discussed in our previous study.[20,23] *E. coli* bacteria (10^7 cfu/mL) and sodium alginate (250
175 mg/L) suspensions were used for accelerated biofouling and fouling experiments, respectively.
176 The fouling experiments were performed for 24 h, the crossflow velocity was set around 8.5
177 cm/s, and the draw solution concentration was slightly adjusted for different membrane samples
178 to obtain the same initial water flux for the various membranes in fouling and biofouling tests.

179 **Evaluation of the Antimicrobial Activity of the Membranes.** *E. coli* (ATCC® 10536™)
180 and *P. aeruginosa* (PA14) bacteria strains were used to evaluate the antibacterial properties of the
181 membranes. A colony of *E. coli* was cultivated overnight (16-17 h) in the LB broth Miller
182 medium (Fisher BioReagents™; Cat. No.: BP9723-2) at 37°C with a stirring rate of 160 rpm. A
183 1:10 dilution of the culture was prepared in phosphate-buffered saline (PBS) with an approximate
184 density of 10^8 cells/mL. 200 µL of the bacteria sample was added onto a 1×1 cm² membrane
185 sample and placed in the dark at room temperature for 3 h. To avoid evaporation of the samples,
186 these were placed in a secondary plate covered with a lid. After the 3 h treatment, samples were
187 stained with 5 µM 4',6-diamidino-2-phenylindole (DAPI, Invitrogen™; Cat. No.: D3571) and 20

188 μM propidium iodide (PI) (Acros Organics; Cat. No.: 440300250) in PBS for 30 min. Each
189 sample was covered by a microscope glass coverslip and epi-fluorescence images were collected
190 by a 40 \times lens (Plan Fluor, 40x/0.75) under an EVOS scope. DAPI and Texas Red channels (70%
191 light intensity; 500 ms exposure time) were used to record the number of live (DAPI-stained) and
192 dead (PI-stained) cells in each FOV. The average percentage of dead cells was determined for at
193 least ten FOVs for each sample.

194 To assess the biofilm inhibition properties of the membranes, a colony of PA14 was
195 cultivated overnight (16-17 hours) in the LB broth Miller medium (Fisher; Cat. No.: BP9723-2)
196 at 37 $^{\circ}\text{C}$ with a stirring rate of 160 rpm. A 1:100 dilution of the culture was prepared in M9
197 minimal medium with an approximate density of 10^7 cells/mL. Five mL of the bacteria sample
198 was added onto a 1 \times 1 cm² membrane samples in a 6-well plate and placed in the dark at room
199 temperature for 48 h. The planktonic bacteria were washed with sufficient PBS and biofilms were
200 then stained with 5 μM DAPI for 30 min in the dark. The excess DAPI was washed with
201 sufficient PBS and epi-fluorescence images were collected with a 10 \times lens to visualize bacteria
202 biofilms. At least ten field of views were examined for each sample.

203 **Chemical Stability of the TFN Membranes.** The chemical stability of the TFN membranes
204 was preliminarily investigated by determining the amount of silver ions released from the TFN
205 membranes. A sample of each membrane (circular sample with a diameter of 2 cm) was stored in
206 20 mL of DI water with continuous shaking (150 rpm) for 30 days. The concentration of silver
207 ions in the DI water solution was determined by inductively coupled plasma mass spectrometry
208 (ICP-MS, AA300 Agilent Technologies).

209 RESULTS & DISCUSSION

210 **Membranes Physiochemical Characterization.** The FTIR spectra (**Figure 2**) of the
211 pristine (blank) membranes and of the membranes prepared with two different concentrations of
212 the MAF-2Imid and MAF-Benz NPs showed a broad peak around 3300 cm^{-1} , representing O–H
213 stretching. [24] The peaks between 1150 and 1320 cm^{-1} detected in all membranes are mostly
214 associated with the PES support: for example, the peak at 1319 cm^{-1} corresponds to O=S=O
215 asymmetric stretching vibration. [20,25,26] The observed peak at 1237 cm^{-1} is assigned to C–O–
216 C symmetric stretching. [26] The band at 1483 cm^{-1} is most likely attributed to C=O stretching
217 vibration present in the amide. [24] The peak associated with N–H stretching was detected at
218 1610 cm^{-1} . [27] The peak at 1575 cm^{-1} is ascribed to N–H bending [27,28] and also C=N
219 stretching present in imidazole structure [29], which is the reason why this peak was more intense
220 for modified membranes. The bands at around 1000 and 1148 cm^{-1} are attributed to the C–N
221 bending and C–N stretching, respectively. [30,31] The peak at 1148 cm^{-1} can also be overlapped
222 by the peak of O=S=O symmetric stretching vibration in the PES. [26] Furthermore, the
223 appearance of a peak with a subtle intensity at around 1543 cm^{-1} is most likely due to possible
224 interactions between NPs and the polyamide network as this peak was not observed in the blank
225 TFC membrane spectrum. [20]

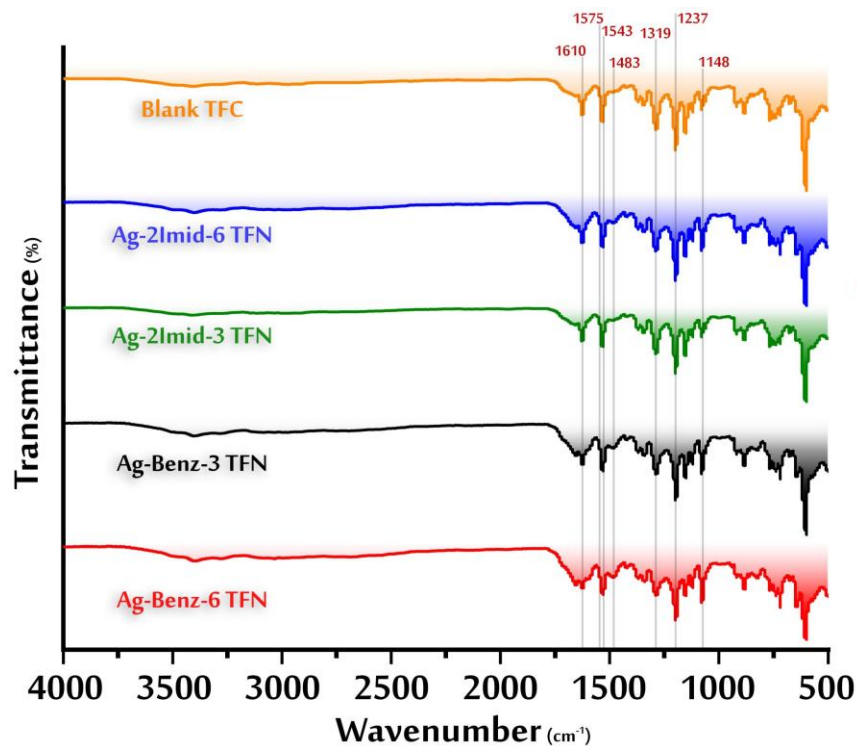


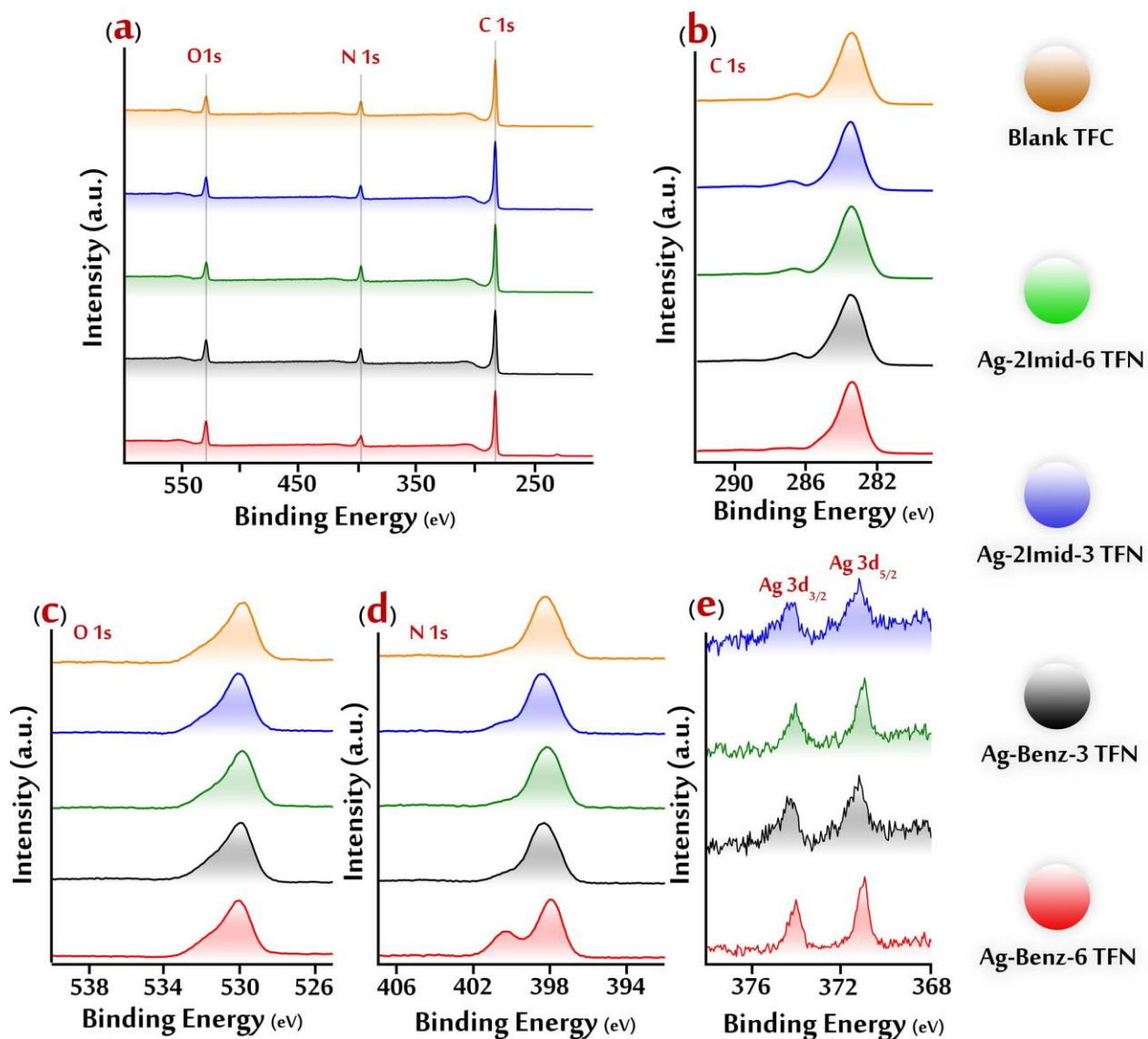
Figure 2. FTIR spectra of membranes.

226
227

228 XPS measurements were performed in order to analyze the elemental composition and
 229 chemical bonds of the membranes (**Figure 3**). High-resolution spectra of modified membranes
 230 showed signals at binding energies of 366 eV (Ag 3d_{5/2}) and 372 eV (Ag 3d_{3/2}), which
 231 corroborate the presence of silver on the modified membranes.[20] The other XPS dominant
 232 peaks are related to carbon, nitrogen, and oxygen (peaks approximately at 283, 398, 530 eV for C
 233 1s, N 1s, and O 1s, respectively), which are observed in all the spectra since these elements are
 234 the PA layer constituents.

235 High-resolution C 1s, N 1s, and O 1s XPS spectra are shown in **Figure 3b-d**. The profiles
 236 related to C 1s indicate two signals in which the major peak centered at 283 is assigned to C–H,
 237 C–C, C=C [32,33], and C-N bonds.[34] The minor peak, approximately at 286 eV, is attributed to
 238 C–O, C-O-C, O-C=O, C-O-H, C=O, and C=N bonds.[20,33] **Figure 3b** shows the deconvoluted
 239 XPS spectra of the O 1s range in which the first peak around 530 eV is attributed to N-C=O, O-

240 C=O, and C=O bonds, and the second peak around 531.5 eV is correlated to O-C=O and C-O-H
241 bonds.[35] In addition, high-resolution XPS spectra of the N 1s region indicate the peak at 398
242 eV, which is mostly attributed to N-H and N-C bonds.[32,34] The N 1s signal of the membrane
243 modified by more concentration of benzimidazole consists of two peaks located approximately at
244 398 and 400 eV (**Figure 3d**). The first peak is additionally assigned to the N atoms in the
245 imidazole ring.[36,37] The second peak appearing for the functionalized membrane and with the
246 higher binding energy is mainly assigned to the nitrogen in the imidazole ring coordinated with
247 silver (N–Ag) [38], which results in the peak shift to higher binding energy. Noticeably, this peak
248 was barely visible in the XPS spectrum of the membrane modified by a lower concentration of
249 benzimidazole; on the other hand, XPS silver atom signals were more intense for the membrane
250 modified by a higher concentration of benzimidazole.



251
 252 **Figure 3.** a) XPS survey spectra of the membranes. Deconvoluted high-resolution XPS spectra of b) C 1s, c) O 1s, d) N
 253 1s, and e) Ag 3d.

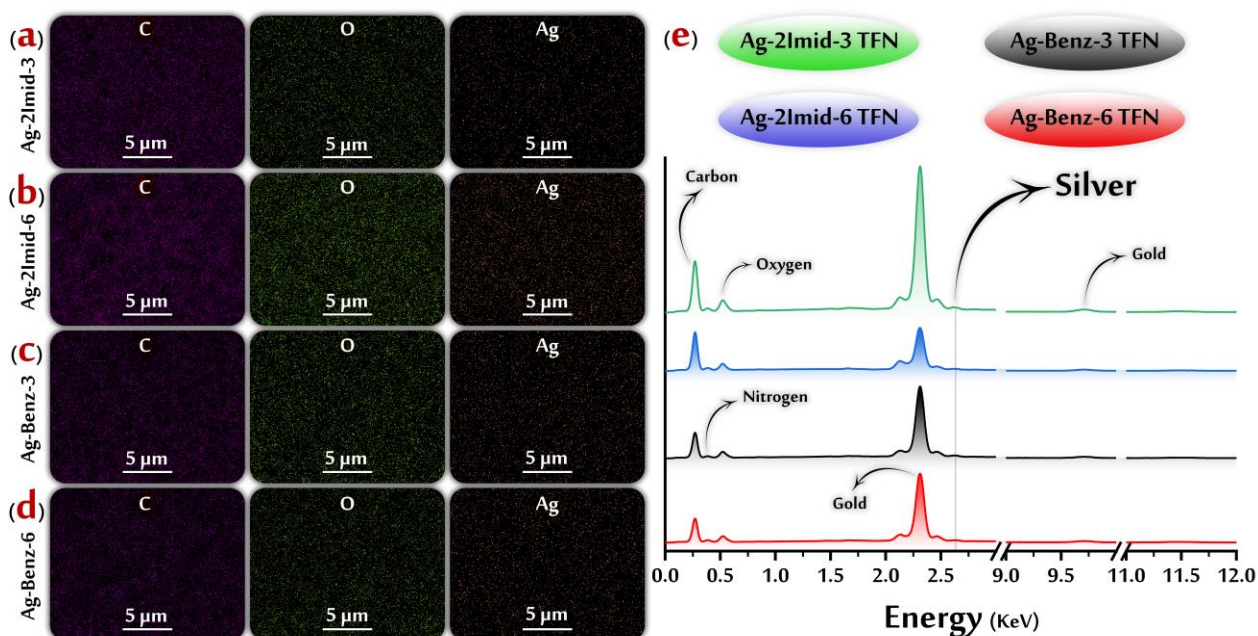
254 **Table 1** summarizes the elemental compositions of the membranes. The O/N ratio of PA
 255 theoretically varies between 1 (fully crosslinked) to 2 (fully linear).[39] The degree of
 256 crosslinking reflects the density of the PA structure and may be correlated to the membrane
 257 selectivity (higher degree of crosslinking should reflect in higher selectivity), whereas a lower
 258 crosslinking may be related to higher hydrophilicity and water flux. **Table 1** also indicates the
 259 ratio of silver atoms peak intensities, from XPS spectra shown in **Figure 3e**, indicating that both

260 Ag-Benz-3 and Ag-Benz-6 TFN membranes had higher concentrations of silver in their
 261 outermost layer than Ag-2Imid-3 and Ag-2Imid-6 TFN membranes, despite the fact that for each
 262 separate pair of TFN membranes the same amount of Ag-MAFs was added during fabrication.
 263 **Figure 4** also shows the relevant EDX spectra and EDX mapping of TFN membranes, clearly
 264 supporting the presence of silver and other relevant atoms at the membrane surface.

265 **Table 1.** O/N ratio, elemental compositions, and Silver atom intensity ratio of the TFC and TFN membranes

Membrane	Atomic concentration (%)				O/N ratio	Ag ratio (from spectra intensity)
	C (1s)	O (1s)	N (1s)	Ag (3d)		
Blank TFC	63.4	21.0	15.6	-	1.3	-
Ag-2Imid-3TFN	61.9	23.0	14.4	0.7	1.6	Ag-2Imid-6/Ag-2Imid-3: 1.2
Ag-2Imid-6-TFN	63.2	20.7	15.2	0.9	1.3	Ag-Benz-3/Ag-2Imid-3: 1.5
Ag-Benz-3 TFN	58.8	24.8	15.4	1.0	1.6	Ag-Benz-6/Ag-Benz-3: 1.4
Ag-Benz-6-TFN	61.8	24.8	12.0	1.4	2.0	Ag-Benz-6/Ag-2Imid-6: 1.8

266



267
268

Figure 4. a-d) Carbon, Oxygen and Silver EDX mapping of TFN membranes, e) EDX spectra of TFN membranes.

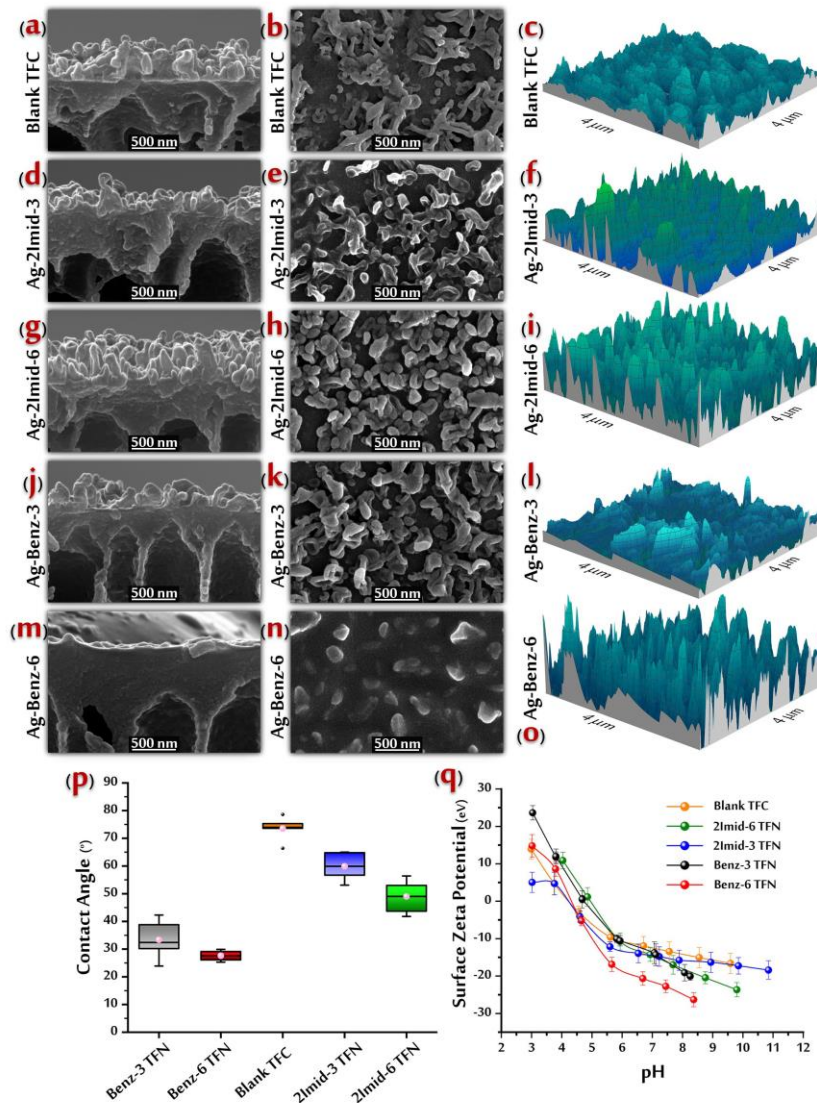
269 SEM cross-sectional and surface micrographs of the TFN membranes are reported in
 270 **Figure 5**. The blank TFC membrane and all TFN membranes exhibited a typical ridge-and-valley
 271 morphology, which is the common structure of PA membranes.[39] Brighter spots can be

272 observed on the surface of TFN membranes upon the incorporation of NPs in the PA layer, which
273 can be attributed to the presence of silver. Such brighter features are more easily detected in the
274 cross-sectional SEM images, especially for the Ag-2Imid-3 TFN membrane. These results may
275 indicate the homogenous and high-density dispersion of the MAF-2Imid and MAF-Benz NPs
276 within the PA layer of modified membranes, supporting the hypothesis of efficient compatibility
277 between NPs and PA matrix.[40] The incorporation of the NPs may decrease the MPD diffusion
278 rate and reduce the polymerization rate of the PA layer as a result of steric hindrance of MAF-
279 2Imid and MAF-Benz NPs.[41] These alterations would, in turn, result in higher water flux.[42]

280 From AFM (**Figure 5**), the average root means square roughness (R_{RMS}) parameter of the
281 membranes was 58, 66, 71, 89, and 103 nm for blank TFC, Ag-2Imid-3, Ag-Benz-3, Ag-2Imid-6,
282 and Ag-Benz-6, respectively. Obviously, the R_{RMS} increased after the addition of NPs, which is
283 consistent with the SEM images of each membrane. This result is especially dominant for Ag-
284 2Imid-6 and Ag-Benz-6 membranes, which have higher contents of NPs and showed larger R_{RMS}
285 values. This observation may support the idea that the higher concentration of NPs ends in
286 agglomerates formation, especially for Ag-Benz TFN membranes.[43] Also, the higher ratio of
287 silver atoms (from XPS spectra) suggests that more NPs exist on the outmost surface of the Ag-
288 Benz TFN membranes, compared with the Ag-2Imid TFN membranes, which may also be a
289 result of non-uniform NPs distribution in the cross-section of the PA layer. This inhomogeneity
290 can affect the performance of the membrane in terms of permeability and selectivity.[44] Also,
291 membranes with rougher surfaces have been reported to be generally more inclined to biofouling
292 by macromolecules and bacterial cells.[23] However, there is no straightforward relationship
293 between fouling behavior, roughness, or hydrophilicity.[11]

294 To assess the surface wettability of the membranes, the water contact angle of the
295 membranes was measured, and results are shown in **Figure 5p**. The average contact angle
296 reduced from 74.1° for the blank TFC membrane to 60.1°, 50.4°, 33.2°, and 28.6° for Ag-2Imid-
297 3, Ag-2Imid-6, Ag-Benz-3, and Ag-Benz-6 TFN membranes, respectively. This improvement in
298 the membrane wettability is attributed to the incorporation of the hydrophilic NPs. Both MAF-
299 2Imid and MAF-Benz NPs contain hydrophilic functional groups on their structure that increase
300 the chance for hydrogen bonds interactions with water molecules.[23] Although all the TFN
301 membranes showed a rougher surface than the blank TFC membrane, wettability may overwhelm
302 the effect of surface roughness in case of biofouling mitigation.[11]

303 Surface charge is another important property of membranes, affecting the rejection of
304 charged contaminants and foulants.[45] Bacterial cells usually carry a negative surface charge in
305 a pH range of 4-9: addition of negatively charged additives can improve the antibiofouling
306 properties of the membranes by exploiting the electrostatic repulsion.[46] **Figure 5q** presents the
307 value of zeta potential for the membranes in the pH range 3-11. The carboxyl groups of the PA
308 layer deprotonate at increasing pH.[47] What stands out in **Figure 5q** is the more negative zeta
309 potential of all the TFN membranes compared to the blank TFC membrane. This result can be
310 attributed to the contribution of functional groups of MAF-2Imid and MAF-Benz present in the
311 structure of NPs. The Ag-Benz-6 TFN membrane was characterized by the largest negative
312 surface charge, which can be attributed to the higher density of MAF-Benz-6 NPs within the
313 active layer and their closer distance from the surface.[48] This improvement in surface charge of
314 all TFN membranes can eventually result in stronger antibiofouling properties.



315
 316 **Figure 5.** a-o) Cross-sectional SEM, top surface SEM, and AFM images of membranes; p) contact angle measurements
 317 of water sitting on the surface of the various membranes; q) zeta potential measurements of the membranes surface.

318 **Biofilm Inhibition and Antibacterial Properties of MAF-enabled Membranes.** The

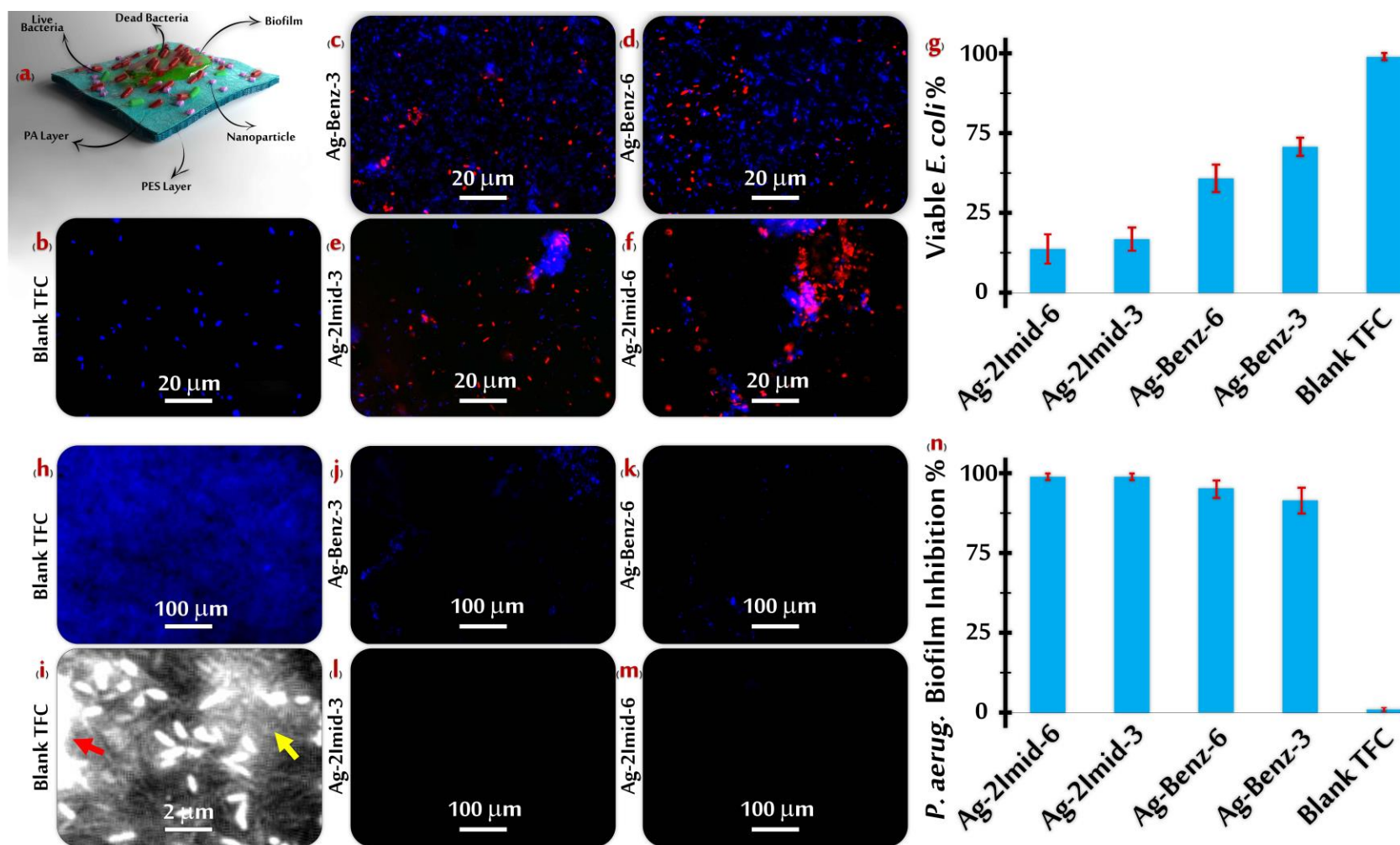
319 effective MAF incorporation into the polyamide active layer is hypothesized to impart
 320 antibacterial properties to the membrane, suitable for biofilm inhibition, and the results of this
 321 assessment are summarized in **Figure 6**. An anti-biofouling membrane should be able to both
 322 inactivate bacterial cells that come into contact with its surface and inhibit the growth and
 323 multiplication of any cells that manage to deposit.

324 To first examine the antibacterial properties of the TFN membranes against planktonic
325 cells, we used *Escherichia coli* (*E. coli*), a common strain with medium to low tendency to make
326 biofilms on surfaces. The viability of bacterial cells upon contact with the membranes was tested
327 by imaging the cells after staining with propidium iodide (PI) and 4',6-diamidino-2-phenylindole
328 (DAPI) molecules. Both fluorophores exhibit fluorescence enhancement upon intercalation into
329 double-stranded regions of DNA (DAPI-stained is blue; PI-stained is red).[49] Considering that
330 the cytoplasmic membrane of bacterial cells is permeable to DAPI but not PI, PI fluorescence
331 enhancement is observed only if the integrity of the cytoplasmic membrane is lost, an indication
332 of the inactivation of bacteria.

333 *E. coli* bacteria, suspended in an aqueous medium, were exposed to the membrane surface
334 for 3 h in the dark to minimize the effect of oxidative stress (e.g., provided by reactive oxygen
335 species).[50,51] While the majority of bacteria (>97%) in contact with the blank TFC membrane
336 were stained only by DAPI molecules (**Figure 6b**), a significant portion of the cells in contact
337 with TFN membranes were stained by PI, indicating their inactivation (**Figure 6c-f**). **Figure 6g**
338 summarizes the percentage of viable *E. coli* cells calculated from these data. Specifically, 60%,
339 47%, 22%, and 18% of the cell population was viable after exposure to Ag-Benz-3, Ag-Benz-6,
340 Ag-2Imid-3, and Ag-2Imid-6 TFN membranes, respectively. Overall, Ag-2Imid membranes
341 showed higher damaging potential toward planktonic *E. coli* compared to Ag-Benz.

342 Furthermore, we examined the ability of the membranes to inhibit the formation of a
343 biofilm by *P. aeruginosa*, a ubiquitous Gram-negative bacterium known for forming robust
344 biofilms.[13,52] As a human opportunistic pathogenic bacterium, *P. aeruginosa* is responsible for
345 both acute and chronic infections, including serious complications in burns, eye lesions, and
346 cystic fibrosis lungs^{2,24-25}. Beside its natural resistance to several drugs²⁸, it is capable of

347 producing strong biofilm structures that facilitate infection and aid the microorganism in
348 withstanding antimicrobial treatment and host defenses³⁰. **Figure 6h** displays a blank TFC
349 membrane that was fully covered by a *P. aeruginosa* biofilm within 48 h. In this experiment,
350 DAPI stained both bacterial cells and extracellular polymeric substances (EPS) within the biofilm
351 structures. Cells and EPS are indicated by a yellow and red arrow, respectively, in **Figure 6i**.
352 TFN membranes, in contrast, provided strong inhibition against biofilm formation. While small
353 pieces of thin biofilms (10-50 μm wide) were observed on Benz- TFN membranes (**Figure 6j**,
354 **and k**), negligible biofilm was present on the 2Imid- TFN membranes (**Figure 6l, and m**).
355 Biofilms were semi-quantitatively determined by measuring the fractional blue area in each field-
356 of-view (FOV): on the basis of this assessment, Ag-Benz-3, Ag-Benz-6, Ag-2Imid-3, and Ag-
357 2Imid-6 TFN membranes resulted in ~90%, 95%, 99%, and 99% inhibition of biofilm formation.
358 Overall, these results corroborated the initial hypothesis: successful incorporation of
359 antimicrobial MAFs provided the membranes with promising antibacterial properties. Similar to
360 *E. coli* results, this effect was more pronounced when deploying MAFs based on the 2-Imidazole
361 ligand.
362



363
364

365

366

Figure 6. (a) Illustration of biofilm formation and mitigation on membranes; (b-f) fluorescence imaging results obtained upon exposure of *E. coli* planktonic cells to the antibacterial membranes. The dead bacteria cells are colored in red while the live bacteria are in blue. (g) Percentage of viable *E. coli* cells; (h-m) *P. aeruginosa* biofilm formed on the membranes. Blue spots represent the biofilm. (n) Resulting percentage of biofilm inhibition by the membranes.

367 **Fouling and Biofouling Effect on Flux Decline.** The static tests discussed above suggest
368 that the membrane surface would act to reduce bacterial growth during operation. However,
369 biofilm formation requires the deposition of cells onto the membrane; a mechanism governed
370 mostly by fluid dynamics and interaction forces (e.g., electrostatic and hydrophobic interactions).
371 Also, bacteria often exploit the pre-deposition of organic foulants to find a hospitable
372 environment at the membrane surface. To gain information on the overall effect of fouling and
373 biofouling on water flux decline, we performed filtration experiments in forward osmosis (FO)
374 configuration and in the presence of alginate or *E. coli* in the feed solution (**Figures 7a and 7b**,
375 respectively). It is worth noting that our preliminary tests suggested a negligible effect of reverse
376 solute passage and draw solution dilution on flux decline. Hence, the observed flux decline in
377 **Figure 7a,b**, might be ascribed solely to fouling-related effects.

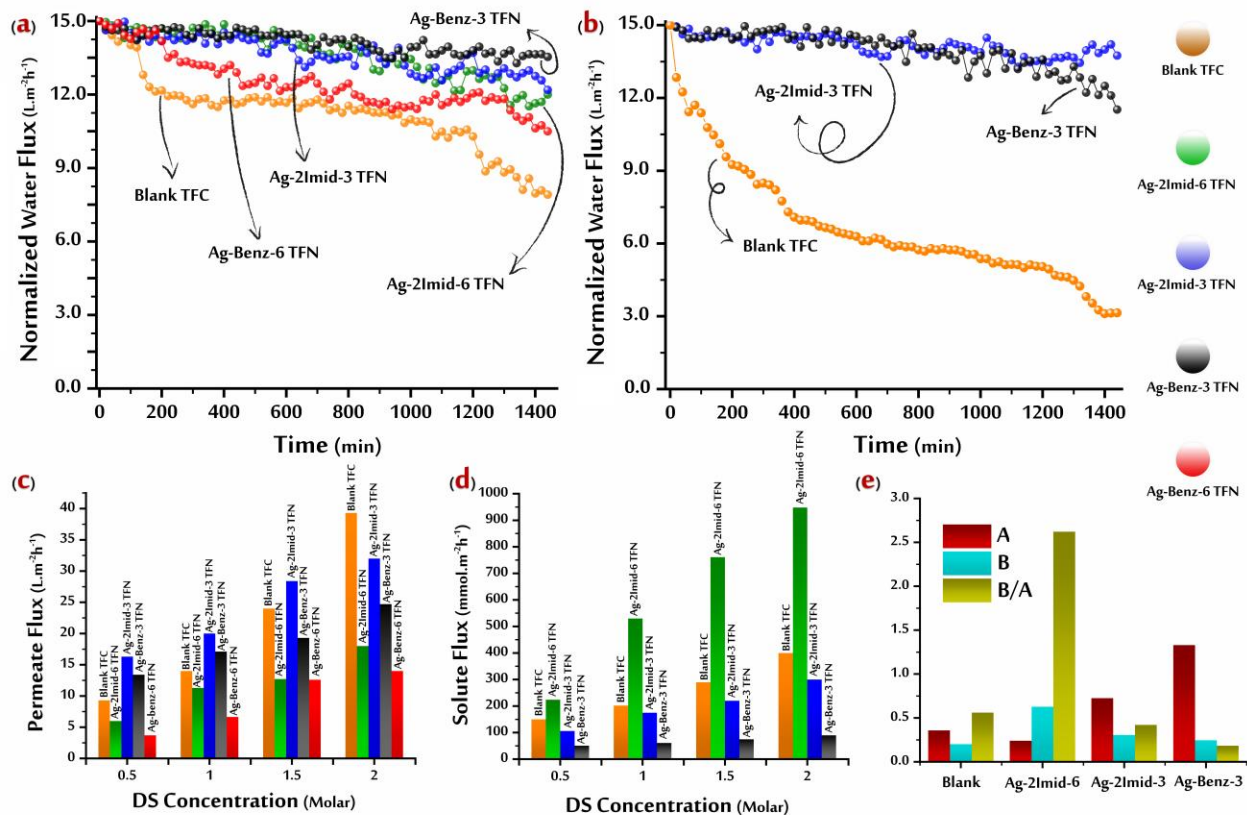
378 As hypothesized, all the TFN membranes showed reduced flux decline compared to the
379 blank TFC membrane. This improvement can be attributed to the combined effects of enhanced
380 wettability of the TFN surfaces (**Figure 5p**) and reduced bacterial growth (**Figure 6**). However,
381 the substantial effect observed in biofouling tests suggests the important role of silver ions in
382 reducing the attachment of the bacterial cells onto the membrane surface and their subsequent
383 growth. TFN membranes improved water flux in tests with sodium alginate and *E. coli* up to
384 approximately 45% and 80%, respectively, with respect to TFC membranes, showing less than
385 10% overall flux decline (especially for bacterial fouling) after 24 h of filtration under accelerated
386 fouling conditions.

387 **Membrane Transport Properties.** The main problem encountered during the fabrication
388 of TFN membranes is the aggregation of nanomaterials that typically cause defects in the
389 synthesized polyamide layer.[63,64] The presence of organic ligands in MAFs can improve their
390 compatibility with the polyamide matrix when compared to other inorganic nanomaterials.[65]

391 One of the main hypotheses of this study is that appropriate MAF chemistry will indeed minimize
392 the deterioration of transport properties or even have a positive impact on flux and rejection
393 performance.

394 The water transport performance of the membranes was studied in a four-step FO
395 protocol[66], and the intrinsic membrane parameters were calculated from water and solute
396 fluxes; see **Figure 7c-e**. The water permeability coefficient, A, increased from 0.3 for blank TFC
397 to 0.7 and 1.3 L m⁻²h⁻¹bar⁻¹ for Ag-2Imid-3 and Ag-Benz-3 TFN membranes, respectively, while
398 the solute permeability coefficient (B) slightly increased from 0.2 to ~0.5 L m⁻²h⁻¹. The water
399 and solute fluxes of the Ag-Benz-6 TFN membrane had large variability and could not be
400 adequately modeled. As a result, the B/A ratio, a parameter that simply indicate the membrane
401 selectivity and that should be as low as possible, decreased for both Ag-2Imid-3 and Ag-Benz-3
402 TFN samples, compared to blank TFC, but it increased for Ag-2Imid-6 TFN, suggesting poor
403 selectivity for the latter membrane. Please note that improvement in selectivity was obtained in
404 combination with an increase in permeance for some membranes, which would result in higher
405 membrane productivity at equivalent or better permeate quality. These results demonstrate
406 improvement in the performance of the TFN membrane, but only in the case of the lesser (0.03%)
407 of the MAF concentrations incorporated during the interfacial polymerization (IP) reaction.

408
409



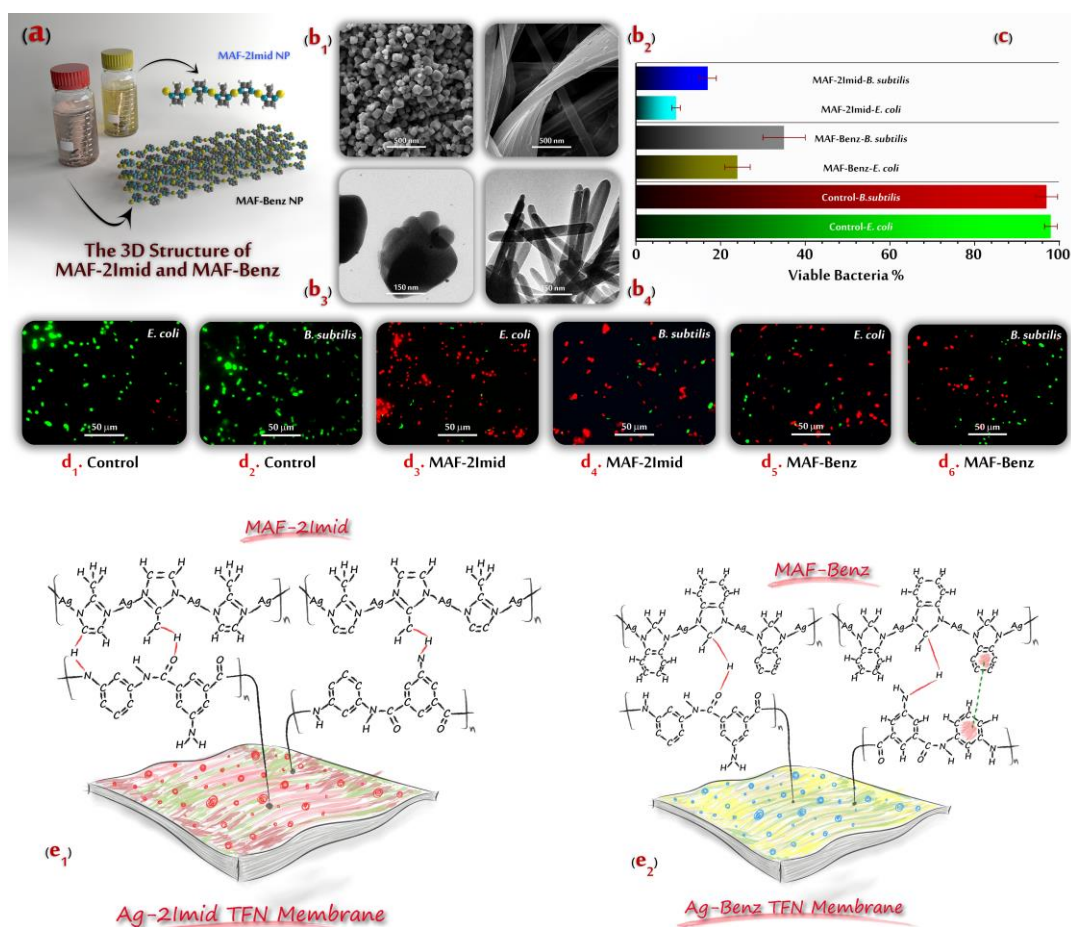
410
 411 **Figure 7.** Membrane transport properties in forward osmosis tests using 1 M NaCl as a draw solution. Flux decline due to (a)
 412 organic fouling by alginate, (b) bacterial fouling by *E. coli*. The results are the average of 3 separate experiments. (c)
 413 Experimental steady-state water flux measured with water as feed solution and a different draw solution concentration for each
 414 measurement step;; (d) experimental steady-state reverse solute flux; resulting (e) transport parameters of the membranes: A
 415 (water permeability coefficient (L m⁻²h⁻¹bar⁻¹)); B (solute permeability coefficient (L m⁻²h⁻¹)). The results are the average of 3
 416 separate experiments.

417 The results reported here demonstrate that functionalization of TFN membranes with
 418 MAF-2Imid and MAF-Benz can inhibit the growth of both planktonic bacteria and the robust
 419 biofilm-forming bacterium *P. aeruginosa*, and mitigate flux decline due to organic fouling and
 420 biofouling. Structure and antimicrobial activity of these MAF NPs are summarized in **Figure 8a-**
 421 **d** and supporting information. MAF-2Imid showed an octahedral structure with an average
 422 particle size of around 760 nm and thickness of MAF-Benz nanoribbons in the range 160-190
 423 nm, with an average particle size of 550 nm. TEM and FE-SEM results of these nanoparticles are
 424 consistent with the assumptions regarding their 3D structure. As with other types of nano-
 425 additives, surface modification with MAFs alters the polyamide layer structure based on one or

426 more of the following three mechanisms; I) changing the kinetics of IP reaction, II) interaction of
427 nanofillers with the PA matrix and affecting the network and aggregate pores, and III) alterations
428 in the hydrolysis degree of acid chloride.[67] Concerning the first mechanism, the presence of
429 nanoparticles during IP may change the penetration rate of TMC/MPD monomers into the
430 reaction zone, and a looser layer may form.[68] This mechanism may be controlled by suitable
431 dispersion of the nanoparticles in the monomer solutions and by adopting appropriate
432 concentrations. The second and third mechanisms may be controlled by careful choice of the
433 organic linker of the nanostructures. Good compatibility with the surrounding polyamide will
434 allow the formation of a seamless selective layer, enabling the MAFs to be incorporated without
435 adverse effects on permeation properties. The rationale is that the organic linker should be chosen
436 to interact with the polyamide chains during membrane formation and in the final layer, thus
437 minimizing defects and discontinuities in the membrane active film. In this study, the methyl and
438 amine functional groups on the surface of MAF-2Imid and MAF-Benz NPs, respectively, most
439 likely interacted with amine and carbonyl/carboxyl groups of the PA layer, along with possible π -
440 π interaction of PA benzene rings with MAF-Benz NPs.[69,70] These chemical interactions
441 would be expected to improve the compatibility and dispersion of MAF-2Imid and MAF-Benz in
442 the PA matrix. **Figure 8e1**, and **8e2** illustrates possible chemical interactions between these two
443 NPs and the PA chains.

444 The better biofouling inhibition and bacterial inactivation observed with Ag-2Imid
445 membranes are consistent with our observations of NP antibacterial performance shown in
446 **Figure 8c and d**, implying that MAF-2Imid nanoparticles have higher intrinsic antibacterial
447 activity compared too MAF-Benz particles. This result can be explained by the intrinsic
448 antimicrobial properties of the imidazole ligand.[22] This molecule can enter the living bacterial

449 cells by passive diffusion and produce nitro radical anions, which can, in turn, oxidize the DNA
 450 or rupture the cell wall to cause the damage and death of the cell.[22] Another hypothesis
 451 suggests that the imidazole rings interact with the flavohaemoglobins present in the bacterial cells
 452 and inhibit the nitric oxide dioxygenase function, thus preventing the metabolism of nitric acid
 453 leading to the death of the cells.[22] That being said, in the case of MAF-Benz and MAF-2Imid
 454 nanoparticles containing silver, the dominant role in antimicrobial activity may be attributed to
 455 silver, and possibly to the coordination ability of silver ions to O, N, or S donor atoms, as well as
 456 hydroxyl, carboxyl, sulfhydryl, and amino functional groups available in the bacterial cell
 457 membrane or DNA, leading to inhibition of bacterial functions.[22]

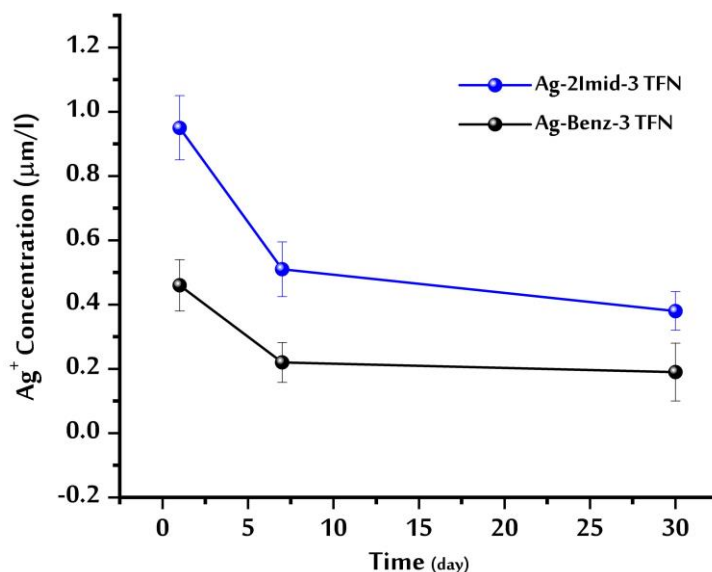


458
 459 **Figure 8.** Schematic illustration of 3D structures and characteristics of MAF-Benz and MAF-2Imid
 460 nanoparticles: b₁) SEM images of MAF-2Imid, b₂) SEM images of MAF-Benz, b₃) TEM image of MAF-2Imid, b₄) TEM

461 image of MAF-Benz, c) antibacterial activity of MAF-Benz and MAF-2Imid particles against *E. coli* and *B. subtilis* and d1-
462 d7) related fluorescence imaging. The dead bacteria cells are colored in red and live bacteria in green. Reproduced with
463 permission from ACS.[22] Schematic illustration of membranes surface chemistry and possible interactions of the metal
464 azolate frameworks with polyamide.

465 A promising feature of TFN membranes is their potential to prevent biofilm growth
466 during long-term operation. MAF-2Imid and MAF-Benz particles may act as reservoirs of silver,
467 promoting the sustained and gradual leaching of this metal ion to achieve prolonged antibacterial
468 activity of the membrane (**Figure 9**). The bacterial inactivation rate may be correlated with the
469 release rate of silver ions. However, a suitable balance should be found between silver-mediated
470 antibacterial activity (i.e., leaching rate) and long-term functionality. To provide insight into this
471 feature, silver leaching tests were carried out for a period of 30 days with both Ag-2Imid-3 and
472 Ag-Benz-3 TFN membranes. Both membranes presented the same trend of the initial decrease in
473 ion release rate for the first 7 days (**Figure 9**). The samples showed a similar behavior
474 characterized by an overall low leaching rate, with this mechanism being slightly faster for the
475 Ag-2Imid-3 TFN membrane. The slow release observed for the membranes allows prolonged
476 antibacterial properties during operation, while providing sufficient activity to inhibit bacterial
477 proliferation, as suggested by the results presented in **Figure 6**. It is important to clarify that
478 membrane antibacterial activity may not directly translate into lower flux decline during
479 filtration. Bacterial growth is only one of the steps involved in biofilm formation, the foremost
480 being attachment of bacteria and other foulants onto the membrane surface. Therefore, preventing
481 this initial seeding phenomenon is also essential. While analogous flux decline was observed with
482 Ag-2Imid-3 and Ag-Benz-3 TFN membranes in the presence of biofoulants, the latter showed
483 reduced flux decline in the presence of alginate, probably due to the improved wettability of its

484 surface, another critical issue provided by the presence of the MAF structures deployed in this
485 study.

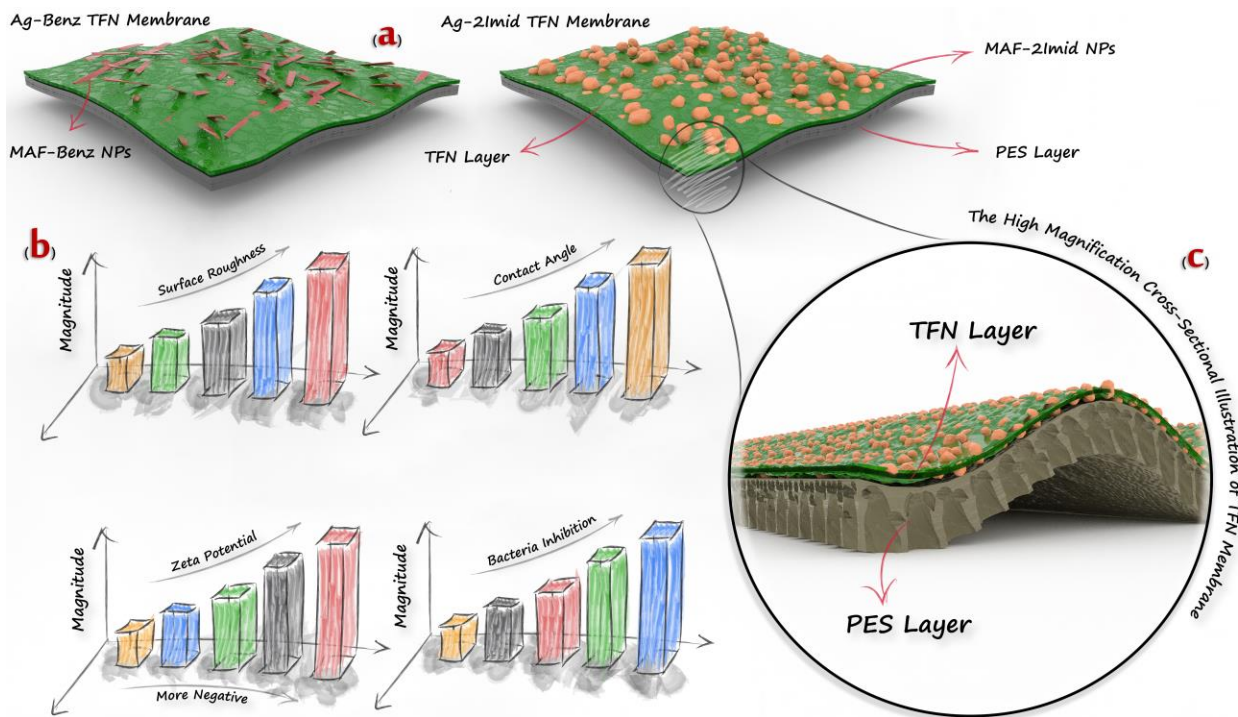


486
487 **Figure 9.** The release rate of Silver ion measured by ICP-MS for a period of 30 days.

488 In terms of membrane transport performance, an advantageously lower B/A ratio was
489 observed for Ag-2Imid-3 and Ag-Benz-3 TFN membranes, together with larger water fluxes
490 compared to the blank TFC membrane (**Figure 7**).[71] This improvement in transport properties
491 may be attributed to the I) improvement in the hydrophilicity of TFN membranes, II) formation
492 of nano-sized voids at the interface of NPs and PA matrix, and III) favorable modification of the
493 morphology and structure (e.g., thickness, density, homogeneity) of the overall active layer in the
494 presence of MAF NPs during membrane synthesis. The formation of large NP aggregates and
495 their inhomogeneous distribution into the PA layer would lead to weak compatibility and
496 reduction in the membrane performance.[72] While increasing the concentration of NPs in the
497 membrane could possibly increase the bactericidal potential (**Figure 6**), increasing MAF
498 concentration has potential disadvantages for PA layer formation, transport properties and costs.
499 Lower MAF concentrations are likely to reduce NP agglomeration, enabling more even

500 distribution of MAFs, more consistent PA layer formation, and possibly superior transport
501 properties.

502 **Figure 10a**, and **c** schematically represents the possible 3D structure of TFN membranes
503 along with the possible key factors affecting their long term performance (**Figure 10b**). The four
504 parameters are well-documented to affect membrane fouling. Higher wettability and electrostatic
505 repulsion minimize the rate of bacterial attachment; increased inhibition of planktonic bacteria
506 decreases the adhesion rate of bacteria on the membrane surface of membrane, further decreasing
507 the chance of fouling. Unlike these three factors, a change in surface roughness can have either
508 positive and negative effects on transport; rougher surfaces may provide more surface available
509 for water passage but it is important to note that the rougher surfaces characterizing TFN
510 membranes may partly thwart the positive effects of surface wettability and promote some
511 deposition of foulants onto the surface depressions of the resulting layer. **Similar to MPD**
512 **monomers, both MAF-2Imid and MAF-Benz nanoparticles carry amine functional groups. These**
513 **groups likely react with the TMC monomers during layer formation, and some additional**
514 **hydrogen and covalent bonds form between NPs and PA chains. Their compatibility is indirectly**
515 **demonstrated by the low salt flux, indicating no or negligible defects in the layer. The durability**
516 **of the TFN membrane was instead investigated by monitoring the silver ion release for 30 days to**
517 **support this hypothesis. The results of the experiments suggest the suitable integrity and**
518 **prolonged antimicrobial activity of the TFN membranes.**



519
 520 **Figure 10.** (a) Schematic illustration of TFN membranes and (b) contributing parameters to antifouling and anti-
 521 biofouling performance; (c) high magnification cross-sectional illustration of TFN membranes. Blue: Ag-2Imid-3,
 522 Green:Ag-2Imid-6, Black: Ag-Benz-3, Red: Ag-Benz-6, and Orange: Blank TFC.

523 **CONCLUSION**

524 Here we provide the first demonstration of a functionalized PA membrane that
 525 simultaneously can maintain high selectivity, achieve almost complete suppression of the growth
 526 of a robust biofilm forming bacterium, inactivation of planktonic bacteria, and retain flux under
 527 the simulation of long-term organic fouling and biofouling. The best improvements were actually
 528 achieved with low concentrations of modifying agents, specifically, only 0.03% mass of
 529 additives, and little generation of hazardous waste products, demonstrating that low-cost and
 530 environmentally benign functionalization can greatly enhance PA membrane performance. The
 531 membranes with 0.03% MAFs (Ag-2Imid-3 and Ag-Benz-3) yielded the best performance.

532 Therefore, further research is needed to determine the ideal concentrations to optimize
533 performance for various applications, feed solutions and performance goals.

534

535 **References**

- 536 [1] J.W. Costerton, Z. Lewandowski, D.E. Caldwell, D.R. Korber, H.M. Lappin-Scott,
537 Microbial biofilms, *Annu. Rev. Microbiol.* 49 (1995) 711–745.
- 538 [2] L. Hall-Stoodley, J.W. Costerton, P. Stoodley, Bacterial biofilms: from the natural
539 environment to infectious diseases, *Nat. Rev. Microbiol.* 2 (2004) 95–108.
- 540 [3] J.J. Harrison, H. Ceri, R.J. Turner, Multimetal resistance and tolerance in microbial
541 biofilms, *Nat. Rev. Microbiol.* 5 (2007) 928–938.
- 542 [4] T.-F. Mah, B. Pitts, B. Pellock, G.C. Walker, P.S. Stewart, G.A. O’toole, A genetic basis
543 for *Pseudomonas aeruginosa* biofilm antibiotic resistance, *Nature.* 426 (2003) 306–310.
- 544 [5] WHO, WHO Publishes List of Bacteria for Which New Antibiotics Are Urgently Needed.
545 Geneva: World Health Organization, (2017).
- 546 [6] D. Davies, Understanding biofilm resistance to antibacterial agents, *Nat. Rev. Drug*
547 *Discov.* 2 (2003) 114–122.
- 548 [7] K. Rupel, L. Zupin, G. Ottaviani, I. Bertani, V. Martinelli, D. Porrelli, S. Vodret, R.
549 Vuerich, D. Passos da Silva, R. Bussani, S. Crovella, M. Parsek, V. Venturi, R. Di
550 Lenarda, M. Biasotto, S. Zacchigna, Blue laser light inhibits biofilm formation in vitro and
551 in vivo by inducing oxidative stress, *Npj Biofilms Microbiomes.* 5 (2019) 29.
552 <https://doi.org/10.1038/s41522-019-0102-9>.
- 553 [8] V. Kochkodan, N. Hilal, A comprehensive review on surface modified polymer
554 membranes for biofouling mitigation, *Desalination.* 356 (2015) 187–207.
- 555 [9] N. Bazrafshan, M.D. Firouzjaei, M. Elliott, A. Moradkhani, A. Rahimpour, Preparation
556 and modification of low-fouling ultrafiltration membranes for cheese whey treatment by
557 membrane bioreactor, *Case Stud. Chem. Environ. Eng.* (2021) 100137.
- 558 [10] H.-C. Flemming, G. Schaule, T. Griebe, J. Schmitt, A. Tamachkiarowa, Biofouling—the

- 559 Achilles heel of membrane processes, *Desalination*. (1997). <https://doi.org/10.1016/S0011->
560 9164(97)00132-X.
- 561 [11] M.D. Firouzjaei, S.F. Seyedpour, S.A. Aktij, M. Giagnorio, N. Bazrafshan, A.
562 Mollahosseini, F. Samadi, S. Ahmadalipour, F.D. Firouzjaei, M.R. Esfahani, Recent
563 advances in functionalized polymer membranes for biofouling control and mitigation in
564 forward osmosis, *J. Memb. Sci.* 596 (2020) 117604.
- 565 [12] M. Elimelech, W.A. Phillip, The future of seawater desalination: energy, technology, and
566 the environment, *Science* (80-.). 333 (2011) 712–717.
- 567 [13] B. Meyer, Approaches to prevention, removal and killing of biofilms, *Int. Biodeterior.*
568 *Biodegradation.* 51 (2003) 249–253.
- 569 [14] H.J. de Vries, F. Beyer, M. Jarzembowska, J. Lipińska, P. van den Brink, A. Zwijnenburg,
570 P.H.A. Timmers, A.J.M. Stams, C.M. Plugge, Isolation and characterization of
571 *Sphingomonadaceae* from fouled membranes, *Npj Biofilms Microbiomes.* 5 (2019) 1–9.
- 572 [15] B. Khorshidi, I. Biswas, T. Ghosh, T. Thundat, M. Sadrzadeh, Robust fabrication of thin
573 film polyamide-TiO₂ nanocomposite membranes with enhanced thermal stability and
574 anti-biofouling propensity, *Sci. Rep.* 8 (2018) 1–10.
- 575 [16] M. Herzberg, M. Elimelech, Biofouling of reverse osmosis membranes: Role of biofilm-
576 enhanced osmotic pressure, *J. Memb. Sci.* 295 (2007) 11-20.
577 <https://doi.org/10.1016/j.memsci.2007.02.024>.
- 578 [17] S.F. Seyedpour, M. Dadashi Firouzjaei, A. Rahimpour, E. Zolghadr, A. Arabi Shamsabadi,
579 P. Das, F. Akbari Afkhami, M. Sadrzadeh, A. Tiraferri, M.A. Elliott, Toward Sustainable
580 Tackling of Biofouling Implications and Improved Performance of TFC FO Membranes
581 Modified by Ag-MOFs Nanorods, *ACS Appl. Mater. Interfaces.* 8 (2020) 7588-7599.

- 582 [18] C. Liu, A.F. Faria, J. Ma, M. Elimelech, Mitigation of biofilm development on thin-film
583 composite membranes functionalized with zwitterionic polymers and silver nanoparticles,
584 Environ. Sci. Technol. 51 (2017) 182–191.
- 585 [19] M. Pejman, M. Dadashi Firouzjaei, S. Aghapour Aktij, P. Das, E. Zolghadr, H. Jafarian, A.
586 Arabi Shamsabadi, M. Elliott, M. Sadrzadeh, M. Sangermano, In Situ Ag-MOF Growth on
587 Pre-Grafted Zwitterions Imparts Outstanding Antifouling Properties to Forward Osmosis
588 Membranes, ACS Appl. Mater. Interfaces. 12 (2020) 36287–36300.
- 589 [20] M.D. Firouzjaei, A.A. Shamsabadi, S.A. Aktij, S.F. Seyedpour, M. Sharifian Gh, A.
590 Rahimpour, M.R. Esfahani, M. Ulbricht, M. Soroush, Exploiting synergetic effects of
591 graphene oxide and a silver-based metal–organic framework to enhance antifouling and
592 anti-biofouling properties of thin-film nanocomposite membranes, ACS Appl. Mater.
593 Interfaces. 10 (2018) 42967–42978.
- 594 [21] H. Erer, O.Z. Yeşilel, C. Darcan, O. Büyükgüngör, Synthesis, spectroscopic, thermal
595 studies, antimicrobial activities and crystal structures of Co (II), Ni (II), Cu (II) and Zn
596 (II)-orotate complexes with 2-methylimidazole, Polyhedron. 28 (2009) 3087–3093.
- 597 [22] S.F. Seyedpour, A. Arabi Shamsabadi, S. Khoshhal Salestan, M. Dadashi Firouzjaei, M.
598 Sharifian Gh, A. Rahimpour, F. Akbari Afkhami, M. reza Shirzad Kebria, M.A. Elliott, A.
599 Tiraferri, Tailoring the Biocidal Activity of Novel Silver-Based Metal Azolate
600 Frameworks, ACS Sustain. Chem. Eng. (2020).
- 601 [23] A. Rahimpour, S.F. Seyedpour, S. Aghapour Aktij, M. Dadashi Firouzjaei, A. Zirehpour,
602 A. Arabi Shamsabadi, S. Khoshhal Salestan, M. Jabbari, M. Soroush, Simultaneous
603 Improvement of Antimicrobial, Antifouling, and Transport Properties of Forward Osmosis
604 Membranes with Immobilized Highly-Compatible Polyrhodanine Nanoparticles, Environ.

- 605 Sci. Technol. (2018) acs.est.8b00804. <https://doi.org/10.1021/acs.est.8b00804>.
- 606 [24] J. Yin, G. Zhu, B. Deng, Graphene oxide (GO) enhanced polyamide (PA) thin-film
607 nanocomposite (TFN) membrane for water purification, *Desalination*. 379 (2016) 93–101.
608 <https://doi.org/10.1016/j.desal.2015.11.001>.
- 609 [25] B. Khorshidi, T. Thundat, B.A. Fleck, M. Sadrzadeh, Thin film composite polyamide
610 membranes: parametric study on the influence of synthesis conditions, *RSC Adv.* 5 (2015)
611 54985–54997.
- 612 [26] X. Wei, Z. Wang, J. Wang, S. Wang, A novel method of surface modification to
613 polysulfone ultrafiltration membrane by preadsorption of citric acid or sodium bisulfite,
614 *Memb. Water Treat.* 3 (2012) 35–49.
- 615 [27] M.I. Baig, P.G. Ingole, W.K. Choi, J. Jeon, B. Jang, J.H. Moon, H.K. Lee, Synthesis and
616 characterization of thin film nanocomposite membranes incorporated with surface
617 functionalized Silicon nanoparticles for improved water vapor permeation performance,
618 *Chem. Eng. J.* 308 (2017) 27–39.
- 619 [28] B. Das, S.K. Dash, D. Mandal, T. Ghosh, S. Chattopadhyay, S. Tripathy, S. Das, S.K. Dey,
620 D. Das, S. Roy, Green synthesized silver nanoparticles destroy multidrug resistant bacteria
621 via reactive oxygen species mediated membrane damage, *Arab. J. Chem.* 10 (2017) 862–
622 876.
- 623 [29] Y. Zhang, Y. Jia, L. Hou, Synthesis of zeolitic imidazolate framework-8 on polyester fiber
624 for PM 2.5 removal, *RSC Adv.* 8 (2018) 31471–31477.
- 625 [30] L. Sarango, J. Benito, I. Gascón, B. Zornoza, J. Coronas, Homogeneous thin coatings of
626 zeolitic imidazolate frameworks prepared on quartz crystal sensors for CO₂ adsorption,
627 *Microporous Mesoporous Mater.* 272 (2018) 44–52.

- 628 [31] D. Huang, Q. Xin, Y. Ni, Y. Shuai, S. Wang, Y. Li, H. Ye, L. Lin, X. Ding, Y. Zhang,
629 Synergistic effects of zeolite imidazole framework@ graphene oxide composites in
630 humidified mixed matrix membranes on CO₂ separation, *RSC Adv.* 8 (2018) 6099–6109.
- 631 [32] C.D. Wagner, A. V Naumkin, A. Kraut-Vass, J.W. Allison, C.J. Powell, J.R. Rumble Jr,
632 NIST X-ray Photoelectron Spectroscopy Database, NIST Standard Reference Database 20,
633 Version 3.4 (Web Version), U. S. Dep. Commer. (2003).
- 634 [33] Z. Liu, J. Ou, H. Wang, X. You, M. Ye, Synthesis and characterization of hydrazide-linked
635 and amide-linked organic polymers, *ACS Appl. Mater. Interfaces.* 8 (2016) 32060–32067.
- 636 [34] Y. Sun, J. Hu, S. An, Q. Zhang, Y. Guo, D. Song, Q. Shang, Selective esterification of
637 glycerol with acetic acid or lauric acid over rod-like carbon-based sulfonic acid
638 functionalized ionic liquids, *Fuel.* 207 (2017) 136–145.
- 639 [35] S. Kim, Y.S. Yun, Y.E. Choi, Development of waste biomass based sorbent for removal of
640 cyanotoxin microcystin-LR from aqueous phases, *Bioresour. Technol.* 247 (2018) 690–
641 696. <https://doi.org/10.1016/j.biortech.2017.09.164>.
- 642 [36] H. Zarrok, A. Zarrouk, B. Hammouti, R. Salghi, C. Jama, F. Bentiss, Corrosion control of
643 carbon steel in phosphoric acid by purpald–weight loss, electrochemical and XPS studies,
644 *Corros. Sci.* 64 (2012) 243–252.
- 645 [37] Z. Cao, Y. Tang, H. Cang, J. Xu, G. Lu, W. Jing, Novel benzimidazole derivatives as
646 corrosion inhibitors of mild steel in the acidic media. Part II: Theoretical studies, *Corros.*
647 *Sci.* 83 (2014) 292–298.
- 648 [38] A.C. Dhayagude, N. Maiti, A.K. Debnath, S.S. Joshi, S. Kapoor, Metal nanoparticle
649 catalyzed charge rearrangement in selenourea probed by surface-enhanced Raman
650 scattering, *RSC Adv.* 6 (2016) 17405–17414.

- 651 [39] J. Benavente, M.I. Vázquez, Effect of age and chemical treatments on characteristic
652 parameters for active and porous sublayers of polymeric composite membranes, *J. Colloid*
653 *Interface Sci.* 273 (2004) 547–555.
- 654 [40] M. Sadeghi, A.A. Shamsabadi, A. Ronasi, A.P. Isfahani, M. Dinari, M. Soroush,
655 Engineering the dispersion of nanoparticles in polyurethane membranes to control
656 membrane physical and transport properties, *Chem. Eng. Sci.* 192 (2018) 688–698.
- 657 [41] X. Song, Q. Zhou, T. Zhang, H. Xu, Z. Wang, Pressure-assisted preparation of graphene
658 oxide quantum dot-incorporated reverse osmosis membranes: antifouling and chlorine
659 resistance potentials, *J. Mater. Chem. A.* 4 (2016) 16896–16905.
660 <https://doi.org/10.1039/C6TA06636D>.
- 661 [42] S. Xia, L. Yao, Y. Zhao, N. Li, Y. Zheng, Preparation of graphene oxide modified
662 polyamide thin film composite membranes with improved hydrophilicity for natural
663 organic matter removal, *Chem. Eng. J.* 280 (2015) 720–727.
- 664 [43] V. Vatanpour, S.S. Madaeni, L. Rajabi, S. Zinadini, A.A. Derakhshan, Boehmite
665 nanoparticles as a new nanofiller for preparation of antifouling mixed matrix membranes,
666 *J. Memb. Sci.* 401 (2012) 132–143.
- 667 [44] C.H. Lau, T.-S. Chung, Effects of Si–O–Si agglomerations on CO₂ transport and
668 separation properties of sol-derived nanohybrid membranes, *Macromolecules.* 44 (2011)
669 6057–6066.
- 670 [45] M. Asadollahi, D. Bastani, S.A. Musavi, Enhancement of surface properties and
671 performance of reverse osmosis membranes after surface modification: a review,
672 *Desalination.* 420 (2017) 330–383.
- 673 [46] A. Zirehpour, A. Rahimpour, S. Khoshhal, M.D. Firouzjaei, A.A. Ghoreyshi, The impact

- 674 of MOF feasibility to improve the desalination performance and antifouling properties of
675 FO membranes, *RSC Adv.* 6 (2016) 70174–70185. <https://doi.org/10.1039/C6RA14591D>.
- 676 [47] A.E. Childress, M. Elimelech, Effect of solution chemistry on the surface charge of
677 polymeric reverse osmosis and nanofiltration membranes, *J. Memb. Sci.* 119 (1996) 253–
678 268.
- 679 [48] M.D. Firouzjaei, F.A. Afkhami, M.R. Esfahani, C.H. Turner, S. Nejati, Experimental and
680 molecular dynamics study on dye removal from water by a graphene oxide-copper-metal
681 organic framework nanocomposite, *J. Water Process Eng.* 34 (2020) 101180.
- 682 [49] C.J.G. Yeh, B.-L. Hsi, W.P. Faulk, Propidium Iodide as a Nuclear Marker in
683 Immunofluorescence. II. Use with Cellular Identification and Viability Studies, *J.*
684 *Immunol. Methods.* 43 (1981) 269–75. [https://doi.org/10.1016/0022-1759\(81\)90174-5](https://doi.org/10.1016/0022-1759(81)90174-5).
- 685 [50] K. Zheng, M.I. Setyawati, D.T. Leong, J. Xie, Antimicrobial Gold Nanoclusters, *ACS*
686 *Nano.* 11 (2017) 6904–10.
- 687 [51] L. Tan, J. Li, X. Liu, Z. Cui, X. Yang, K.W.K. Yeung, H. Pan, Y. Zheng, X. Wang, S. Wu,
688 In Situ Disinfection through Photoinspired Radical Oxygen Species Storage and Thermal-
689 Triggered Release from Black Phosphorous with Strengthened Chemical Stability, *Small.*
690 14 (2018) 1703197.
- 691 [52] R. Sommer, S. Wagner, K. Rox, A. Varrot, D. Hauck, E.-C. Wamhoff, J. Schreiber, T.
692 Ryckmans, T. Brunner, C. Rademacher, Glycomimetic, orally bioavailable LecB inhibitors
693 block biofilm formation of *Pseudomonas aeruginosa*, *J. Am. Chem. Soc.* 140 (2018) 2537–
694 2545.
- 695 [53] P.K. Singh, A.L. Schaefer, M.R. Parsek, T.O. Moninger, M.J. Welsh, E.P. Greenberg,
696 Quorum-Sensing Signals Indicate that Cystic Fibrosis Lungs Are Infected with Bacterial

- 697 Biofilms, *Nature*. 407 (2000) 762–64.
- 698 [54] V.E. Wagner, B.H. Iglewski, P. aeruginosa Biofilms in CF Infection, *Clin. Rev. Allergy*
699 *Immunol.* 35 (2008) 124–34. <https://doi.org/10.1007/s12016-008-8079-9>.
- 700 [55] J.W. Costerton, P.S. Stewart, E.P. Greenberg, Bacterial Biofilms: A Common Cause of
701 Persistent Infections, *Science*. 284 (1999) 1318–22.
- 702 [56] J.B. Lyczak, C.A. Cannon, G.B. Pier, Establishment of *Pseudomonas aeruginosa* Infection:
703 Lessons from a Versatile Opportunist, *Microbes Infect.* 2 (2000) 1051–60.
- 704 [57] A.F. Konings, L.W. Martin, K.J. Sharples, L.F. Roddam, R. Latham, D.W. Reid, I.L.
705 Lamont, *Pseudomonas aeruginosa* Uses Multiple Pathways To Acquire Iron During
706 Chronic Infection in Cystic Fibrosis Lungs, *Infect. Immun.* 81 (2013) 2697–704.
707 <https://doi.org/10.1128/IAI.00418-13>.
- 708 [58] J.F. Fisher, S.O. Meroueh, S. Mobashery, Bacterial Resistance to β -Lactam Antibiotics:
709 Compelling Opportunism, *Compelling Opportunity*, *Chem. Rev.* 105 (2005) 395–424.
- 710 [59] T.R. De Kievit, M.D. Parkins, R.J. Gillis, R. Srikumar, H. Ceri, K. Poole, B.H. Iglewski,
711 D.G. Storey, Multidrug Efflux Pumps: Expression Patterns and Contribution to Antibiotic
712 Resistance in *Pseudomonas aeruginosa* Biofilms, *Antimicrob. Agents Chemother.* 45
713 (2001) 1761–70. <https://doi.org/10.1128/AAC.45.6.1761>.
- 714 [60] L. Ma, M. Conover, H. Lu, M.R. Parsek, K. Bayles, D.J. Wozniak, Assembly and
715 Development of the *Pseudomonas aeruginosa* Biofilm Matrix, *PLoS Pathog.* 5 (2009)
716 e1000354. <https://doi.org/10.1371/journal.ppat.1000354>.
- 717 [61] J. Azeredo, N.F. Azevedo, R. Briandet, N. Cerca, T. Coenye, A.R. Costa, M. Desvaux,
718 G.D. Bonaventura, Etc., Critical Review on Biofilm Methods, *Crit. Rev. Microbiol.* 43
719 (2017) 313–51. <https://doi.org/10.1080/1040841X.2016.1208146>.

- 720 [62] K.M. Colvin, V.D. Gordon, K. Murakami, B.R. Borlee, D.J. Wozniak, G.C.L. Wong, M.R.
721 Parsek, The Pel Polysaccharide Can Serve a Structural and Protective Role in the Biofilm
722 Matrix of *Pseudomonas aeruginosa*, *PLoS Pathog.* 7 (2011) e1001264.
723 <https://doi.org/10.1371/journal.ppat.1001264>.
- 724 [63] M. Pejman, M.D. Firouzjaei, S.A. Aktij, P. Das, E. Zolghadr, H. Jafarian, A.A.
725 Shamsabadi, M. Elliott, M.R. Esfahani, M. Sangermano, Improved antifouling and
726 antibacterial properties of forward osmosis membranes through surface modification with
727 zwitterions and silver-based metal organic frameworks, *J. Memb. Sci.* (2020) 118352.
- 728 [64] M. Pejman, M. Dadashi Firouzjaei, S. Aghapour Aktij, P. Das, E. Zolghadr, H. Jafarian, A.
729 Arabi Shamsabadi, M.A. Elliott, M. Sadrzadeh, M. Sangermano, A. Rahimpour, A.
730 Tiraferri, In-Situ Ag-MOFs Growth on Pre-Grafted Zwitterions Imparts Outstanding
731 Antifouling Properties to Forward Osmosis Membranes, *ACS Appl. Mater. Interfaces.*
732 (2020). <https://doi.org/10.1021/acsami.0c12141>.
- 733 [65] R. Dawson, A.I. Cooper, D.J. Adams, Nanoporous organic polymer networks, *Prog.*
734 *Polym. Sci.* 37 (2012) 530–563.
- 735 [66] A. Tiraferri, N.Y. Yip, A.P. Straub, S.R.-V. Castrillon, M. Elimelech, A method for the
736 simultaneous determination of transport and structural parameters of forward osmosis
737 membranes, *J. Memb. Sci.* 444 (2013) 523–538.
- 738 [67] D.H.N. Perera, Q. Song, H. Qiblawey, E. Sivaniah, Regulating the aqueous phase
739 monomer balance for flux improvement in polyamide thin film composite membranes, *J.*
740 *Memb. Sci.* 487 (2015) 74–82.
- 741 [68] M.E.A. Ali, L. Wang, X. Wang, X. Feng, Thin film composite membranes embedded with
742 graphene oxide for water desalination, *Desalination.* 386 (2016) 67–76.

- 743 <https://doi.org/https://doi.org/10.1016/j.desal.2016.02.034>.
- 744 [69] S. Bano, A. Mahmood, S.-J. Kim, K.-H. Lee, Graphene oxide modified polyamide
745 nanofiltration membrane with improved flux and antifouling properties, *J. Mater. Chem.*
746 *A.* 3 (2015) 2065–2071. <https://doi.org/10.1039/C4TA03607G>.
- 747 [70] N.K. Saha, S. V Joshi, Performance evaluation of thin film composite polyamide
748 nanofiltration membrane with variation in monomer type, *J. Memb. Sci.* 342 (2009) 60–69.
749 <https://doi.org/https://doi.org/10.1016/j.memsci.2009.06.025>.
- 750 [71] W.A. Phillip, J.S. Yong, M. Elimelech, Reverse draw solute permeation in forward
751 osmosis: modeling and experiments, *Environ. Sci. Technol.* 44 (2010) 5170–5176.
- 752 [72] M.L. Lind, A.K. Ghosh, A. Jawor, X. Huang, W. Hou, Y. Yang, E.M. V Hoek, Influence
753 of zeolite crystal size on zeolite-polyamide thin film nanocomposite membranes,
754 *Langmuir.* 25 (2009) 10139–10145.
- 755